Peer reviewed version

License (if available):
CC BY

Link to published version (if available):
https://doi.org/10.1007/978-3-031-37007-6_5

Link to publication record in Explore Bristol Research
PDF-document

University of Bristol - Explore Bristol Research
General rights

Low-Frequency Vibrothermography Using Lightweight Piezoelectric Actuators: The Location of Excitation and Application to Composite Materials

Xintian Chi[1], Dario Di Maio[2], and Nicholas A. J. Lieven[1]

[1] Department of Aerospace Engineering
University of Bristol
Queens Building, University Walk
Bristol, BS8 1TR, UK

[2] Faculty of Engineering Technology
University of Twente
Horst Complex
7522LW Enschede, The Netherlands

ABSTRACT

This article presents a novel infrared thermographic approach for damage detection by utilizing the heat generated around damage sites during vibrations below 1000 Hz induced by lightweight piezoelectric actuators. In this research, the optimal location of excitation was first investigated through finite element analyses, where two generalized equations were obtained to describe the relationship between the excitation and the resulting displacement response. These observations were then verified experimentally on an aerospace-grade composite plate, followed by vibrothermographic tests conducted on the same structure to demonstrate the effectiveness of the proposed damage detection process employing only a single lightweight piezoelectric disc as the actuator.

INTRODUCTION

Vibrothermography is a multi-physics technology that can be applied to non-destructive testing and evaluation, structural health monitoring and characterization of dynamic behavior under long-timescale vibratory motion by exploiting the heat generated between interfaces [1]. When an object is subjected to vibratory excitation, heat will be generated internally through mechanisms such as frictional heating, viscoelastic heating, plasticity-induced heat generation and sometimes thermoelastic effect [2]. The heat generated inside is often caused by damage, defects or other issues and can be conducted to the surfaces and detected by infrared cameras, which can then be used to identify and locate these issues [3–7]. In some literature, this approach is less commonly known by other names such as (ultra)sonic infrared thermography, thermosonics or ultrasonic vibrothermography when acoustic or ultrasonic transducers are used as the excitation sources [7].

For this reason, in vibrothermography, temperature measurement is utilized to read across the mechanics of contact and tribology of interfaces which can change over time because of damage or altered contact conditions. Because of the unique heat generation mechanisms, vibrothermography is especially powerful for detecting a wide variety of problems. In addition, as the damage and defects act as the internal heat sources, the travel distances of heat waves are shortened compared to the case with externally applied heat in conventional active thermography [8], which suggests that vibrothermography is faster and can be particularly helpful for detecting issues at greater depth.

To ensure detectable heat generation, there must be adequate strain energy in relevant regions such as the damage sites [2, 4, 6, 9–26]. For any structure subjected to vibratory excitation, its operating deflection shape (ODS) is a combination of the mode shapes of all the excited modes [27], so obtaining the modal parameters of the structure can provide critical information for understanding its dynamic behaviors, including the strain distributions around the potential damage sites. Based on this comment, to perform vibrothermographic tests effectively, the dynamic properties—specifically modal parameters—of the inspected objects must be analyzed so that the behaviors—in particular the distributions of strain—can be revealed, interpreted and utilized to control the vibrations of the structures [3, 4], which can be achieved through modal analysis.

In analogy to conventional infrared thermography [28], external excitation might or might not be required in order to perform vibrothermographic testing. In most situations, vibrothermography refers to the processes with external excitation provided. Typical examples involve utilizing external excitation in the forms of mechanical forces or ultrasonic waves created by sources such as electrodynamic shakers [29–33] and ultrasonic transducers, where the latter usually include ultrasonic welders [9–11, 34–36] and piezoelectric actuators [11–20, 36–47].

When external excitation is required, to optimize the parameters of a vibrothermographic test, a target mode—or modes—of vibration should be chosen first. After this, parameters related to the excitation of the structure need to be carefully selected to ensure that the right resonance—or resonances—can be excited effectively which can exhibit a viable strain distribution across the structure. The dynamic response with the correct modal distribution will increase the strain in damaged regions so that the heat generation can be increased as well, which enhances the chance of successful detection of damage and defects.

When a single mode of vibration is considered, to excite the target mode effectively, sinusoidal excitation whose frequency matches the corresponding natural frequency should be used. In this case, the structure will exhibit a greater dynamic response and so the heat generation will be increased as well [4, 9–13, 16, 18–22, 26, 37–42, 45–47]. Due to the relationship between heat generation and strain energy, a mode in which the potential damage sites possess high strain energy is preferred.

In vibrothermographic testing, damage and defects often generate more heat in higher-order modes of vibration due to the increased frequencies [21, 22, 33, 47]. However, for high-order modes, issues such as transverse shear and rotary inertia can become more significant, which correspondingly add complexity to the analytical modelling process [47]. In vibrothermographic tests, vibrations in higher-order modes are also usually more localized, so the coverage of strain energy in the test structure can be relatively limited which reduces the effective area of detection. From a practical point of view, more specialized amplifiers are also required for excitation at high frequencies, which may limit the general applicability of this approach. These high-frequency excitation forces may bring other concerns to the test structures because of the high strain rates, with which additional damage may be generated. This last issue is especially problematic for structures made of laminated composite materials, such as the structure studied in this research, which are intrinsically vulnerable to impact or high strain-rate loading [48–53]. As a comparison, vibrothermographic tests targeting lower-order modes may suffer from

issues caused by insufficient heat generation. However, these tests are often easier to apply with fewer practical concerns such as the factors stated above.

In comparison to the frequency of excitation, selecting the optimal location of excitation is not as straightforward and is almost always omitted in relevant research activities. The optimal location of excitation depends on the type of actuator and the method of excitation used. The actuators available for vibrothermographic testing can be approximately grouped into three categories based on the mode of excitation that is provided,

The first category is linear actuators such as electrodynamic shakers [29–33] and longitudinal piezoelectric actuators that can then be subdivided into piezoelectric stack actuators [11, 13, 20, 37–39, 46], bolt-clamped Langevin transducers [17, 19, 44] and piezoelectric shakers [16, 40, 41, 47]. Some other ultrasonic transducers such as ultrasonic welders, when used in vertical alignment, are also examples of this category [54], which have been proven useful for vibrothermographic testing [9–11, 34–36]. To summarize, thanks to the simple mode of excitation, convenient set-up and high amplitudes of the produced forces, linear actuators have been widely utilized in vibration tests, including vibrothermographic inspections.

Alternatively, piezoelectric materials may also be applied as shear actuators. Despite having equally wide frequency ranges, the shear loads achievable are usually significantly lower than the forces produced by the linear actuators. Separately, ultrasonic welders can also be placed parallel to the weld surfaces to induce shear forces into the structures. However, tests using shear actuators are often more difficult to plan and set up while the efficiency of energy transfer is also lower, which limits their practical use in relevant tests.

The third category is the contracting actuators, which typically include lightweight piezoelectric actuators such as piezoelectric discs. These contracting actuators may also be attached to substrates, which can be another piezoelectric material or a passive material such as metal or ceramic, to act as bending actuators [55, 56]. There have been research activities demonstrating the effectiveness of these actuators for vibrothermography [12, 14, 15, 18, 42, 43]. Due to the mode of displacement and the fact that such actuators are often relatively thin and lightweight, the amplitudes of the excitation are often among the lowest compared to alternative options. However, piezoelectric discs and patches can be permanently bonded to or embedded in a structure [14, 15, 42, 43] without causing noticeable modifications to the structure's physical properties. This attribute enables the possibility of easier in-situ damage detection and structural health monitoring. In addition, because of the small size and low weight of these actuators, multiple piezoelectric discs or patches can be attached to a single structure. Activating the actuators simultaneously can increase the response level of the test structure during the induced vibration, which compensates for the low power output of such actuators to some extent.

In this paper, a successful vibrothermographic test was conducted on an aerospace-grade composite plate containing subsurface damage with low-frequency excitation (<1000 Hz) generated using a single lightweight piezoelectric disc, which would provide a high level of convenience and flexibility as explained above. This approach has seldom been applied in either modal tests or vibrothermographic experiments due to the low level of dynamic response. However, in the test to be presented, detectable heat was still able to be generated with carefully selected parameters of excitation.

LOCATION OF EXCITATION

For contracting or bending actuators such as the piezoelectric discs, the selection of the optimal location for excitation in vibrothermography is rarely considered. However, because of the low amplitudes of vibration achievable with these actuators, determining the optimal location of excitation should be optimized to achieve viable dynamic response.

In principle, the analogy to linear actuators can still be applied [55]. In detail, both surface-bonded and embedded piezoelectric actuators should be placed in regions of higher strain to induce greater dynamic responses of the structure [55, 57]. This observation is equally relevant for vibration suppression and control [58]. For a specific mode of vibration, they should be located in regions of high modal strain (energy) to control the vibrations more effectively [59, 60], which means that strain nodal lines should be avoided [61]. When utilized as sensors, these conclusions would still apply [60, 62].

To verify these statements, finite element (FE) analyses were conducted, during which multiple piezoelectric discs were created and attached to a free-free plate. The dynamic responses of the plate when different discs were used to provide the excitation were calculated using direct-solution steady-state dynamic analyses, then recorded and compared so that the relationship between the dynamic response of the structure and the location of excitation could be investigated. The details of the modelling process are thoroughly explained in a separate publication [1].

As shown in **Fig. 1**, the free-free plate model created in Abaqus was composed of a cuboid base and 45 identical piezoelectric discs. Due to the symmetry of the model, the 15 discs in the bottom-left region could be used to represent the behaviors in the other three quarters. For future reference, the 15 discs were named Ai-j, where i represented the row number while j represented the column number. The disc A1-1 corresponded to the disc closest to the bottom-left corner while the disc A3-5 corresponded to the disc at the center of the top surface of the plate.
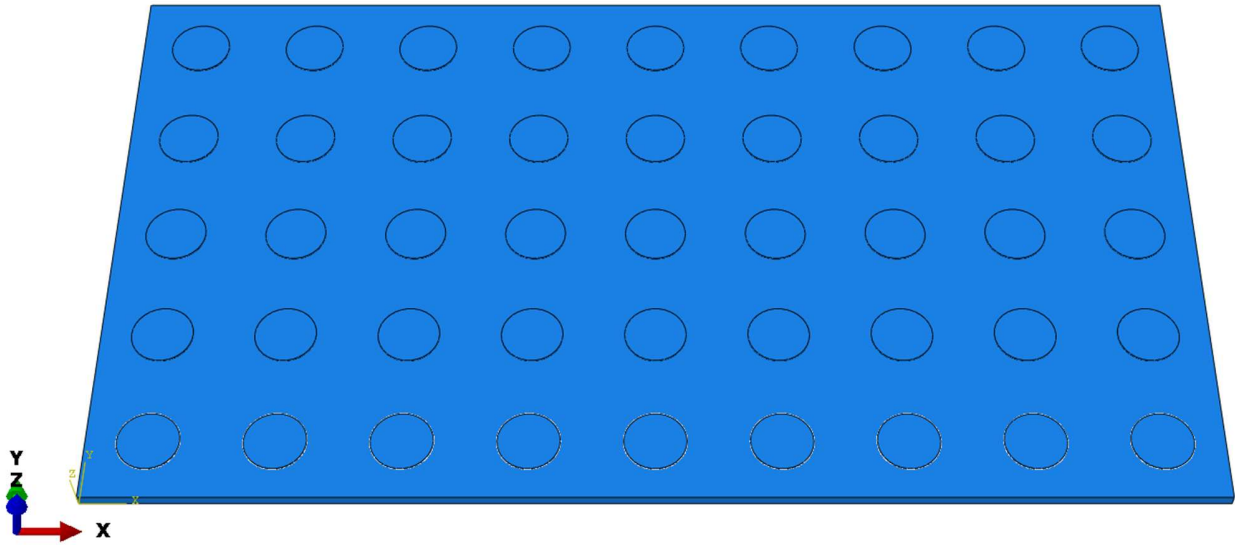

Fig. 1 Free-free plate model created in Abaqus

A natural frequency extraction step was performed first to calculate the modal parameters of the free-free plate model. The natural frequencies and mode shapes of the first four modes of vibration were calculated and recorded. For quantitative data collection, the magnitude of deformation ϕ_{mag} and its three components ϕ_X, ϕ_Y and ϕ_Z, in addition to the six strain components ε_{XX}, ε_{YY}, ε_{ZZ}, ε_{XY}, ε_{XZ} and ε_{YZ}, were extracted at 19 nodes as shown in **Fig. 2**.

To be more specific, the first 15 nodes were located on the top surface of the plate where the centers of the bottom surfaces of the 15 aforementioned discs were attached, which made them the locations of excitation in the subsequent direct-solution steady-state dynamic analyses. Besides these 15 nodes, the four corner nodes of the top surface of the plate were also included. These extracted data would be utilized later to analyze the relationship between the location of excitation and the dynamic response of the model.

Following the completion of the natural frequency extraction step, 24 direct-solution steady-state dynamic analyses were completed to obtain the dynamic responses of the free-free plate model. In the first 15 analyses, each of the 15 discs was subjected to a voltage of 10 V in its direction of polarization. In the next two analyses, discs A2-2 and A2-4 were provided with voltages of 5 V instead, followed by three analyses where discs A3-1, A3-3 and A3-5 were supplied with voltages of 20 V. In the 21st analysis, three different voltages, namely 10 V, 5 V and 20 V, were applied to discs A1-1, A2-2 and A3-3 respectively. In the 22nd analysis, the same voltages were applied to discs A1-3, A2-2 and A3-1. Similarly, discs A1-3, A2-4 and A3-5 were used for the 23rd analysis while discs A1-5, A2-4 and A3-3 were used for the 24th analysis. During the analyses, boundary conditions were applied to maintain the electric potentials at the remaining discs at zero.
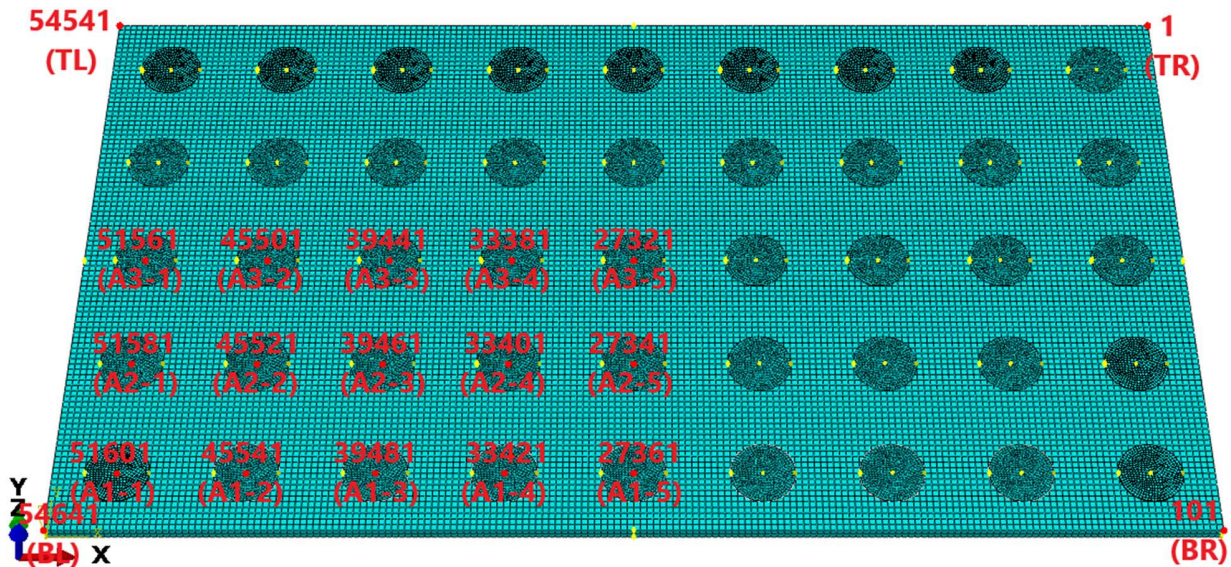
Fig. 2 Locations of the excitation and measurement points on the free-free plate

In each analysis, the steady-state responses of the free-free plate when the frequency (or frequencies) of the voltage (or voltages) matched each of the four natural frequencies of interest were obtained. To demonstrate the results, the deformed shapes of the free-free plate when a voltage of 10 V was applied to disc A1-1 are shown in **Fig. 3**.
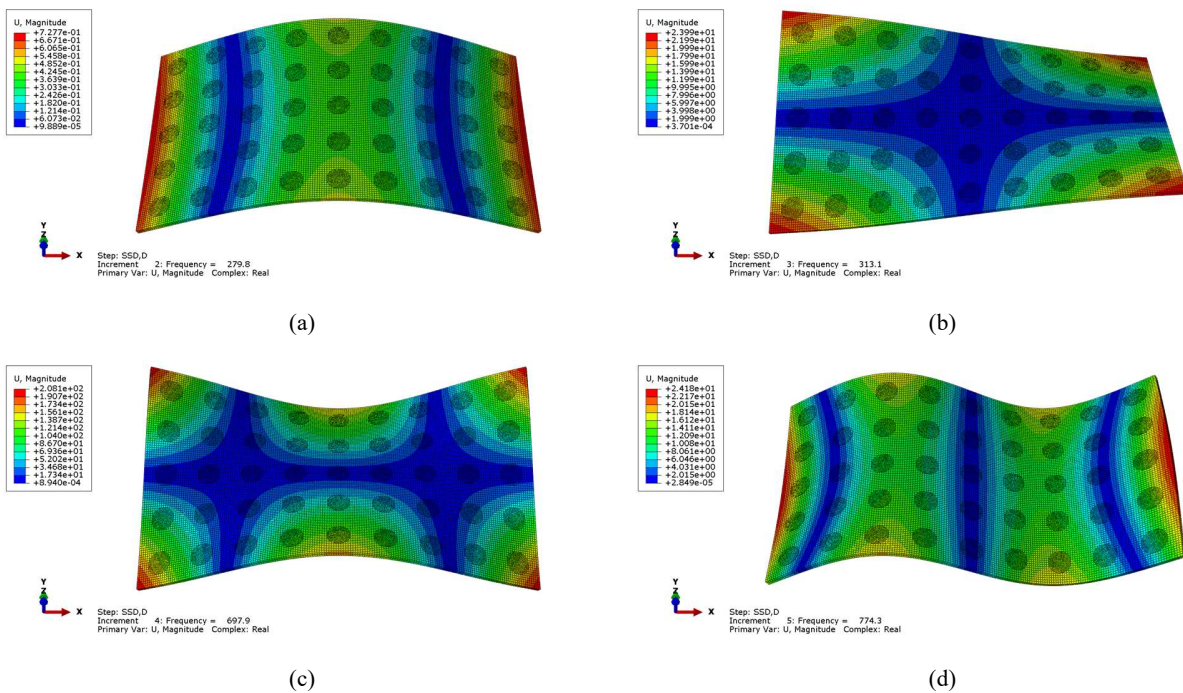

(a)

(b)

(c)

(d)

Fig. 3 Deformed shapes of the free-free plate excited by the piezoelectric disc closest to its bottom-left corner when the frequency of the voltage matched the natural frequencies of the (a)–(d) first to fourth modes of vibration

To record the data, the same 19 nodes were used for quantitative data collection, at which the displacement values were probed to represent the dynamic responses after the direct-solution steady-state dynamic analyses. By analyzing the extracted dynamic response levels with the previously recorded modal parameters, the following relationship was obtained:

$$\mathbf{U}_{\mathrm{resp}} \propto \sum_{j}^{M} AV_Z^j \left(\varepsilon_{XX}^j + \varepsilon_{YY}^j \right) \mathbf{\Phi} , \tag{1}$$

where $\mathbf{U}_{\mathrm{resp}}$ is the displacement response of the structure, M is the number of excitation forces (number of discs in this case), A is a scale factor related to both the properties of the structure, such as damping, and the parameters of the piezoelectric actuator, such as the piezoelectric coefficients, V_Z^j is the voltage applied in the direction of polarization of the jth actuator while ε_{XX}^j and ε_{YY}^j are the first two components of modal strain at the location of excitation.

When several modes of vibration would be excitation, the induced dynamic response of the structure should still be the sum of the individual cases, so equation (1) may be generalized to:

$$\mathbf{U}_{\mathrm{resp}} \propto \sum_{i}^{N} \sum_{j}^{M} A_i V_Z^j \left(\varepsilon_{XX}^{ij} + \varepsilon_{YY}^{ij} \right) \mathbf{\Phi}^i , \tag{2}$$

where A_i now also depends on the difference between the frequency of the voltages and the natural frequency of the ith excited mode. For completeness, the derivation of the equations above is thoroughly explained in a separate publication, together with the recorded quantitative data mentioned above. Similar research was also conducted for electrodynamic shakers representing linear actuators, where generalized equations were also obtained [1].

Based on this research, especially the two generalized equations above, it may be concluded that for contracting or bending actuators, the level of the dynamic response is proportional to the weighted sum of the first two modal strain components at the node where the actuator is attached. When multiple actuators are used, the weighted sum of the modal strain components at all excitation locations should be considered, where the weight is determined by the amplitude of the voltage supplied to each actuator, given that the actuators are all identical.

For more complicated situations that were not discussed in this research, such as when multiple actuators of different types are used together, or when excitation forces no longer have equal frequencies, the proposed relationship will undoubtedly become more complex. However, the observations and conclusions obtained in this research should still be able to act as general guidelines on selecting proper locations of excitation to increase the overall dynamic response of a structure, which is crucial for both conventional vibration testing and vibrothermography.

EXPERIMENTAL VERIFICATION WITH MODAL TESTING

To reiterate, as introduced previously, although there have been research outputs showing the utilization of these piezoelectric actuators in vibrothermography [12, 14, 15, 18, 42, 43], the optimal location of excitation is rarely considered, especially experimentally. This omission can be particularly critical for vibrothermographic tests using piezoelectric discs or patches due to their low power output. In addition, in previous research activities using piezoelectric actuators, high-frequency (ultrasonic) excitation has been predominantly employed. For these reasons, this research was conducted focusing on vibrothermographic testing with lightweight low-power piezoelectric discs using low excitation frequency.

The specimen to be studied was an aerospace-grade composite plate as shown in **Fig. 4**(a). The plate was made of HexPly® 8552 epoxy matrix AS4 fiber woven carbon prepregs containing delamination along the vertical centerline of the plate created artificially through dynamic fatigue. Ply drops were added during the manufacturing phase to help create the damage. The damage was subsurface and barely visible from visual inspection. Due to the subtlety of the damage and the potential lack of energy because of the low-power actuators, the parameters of excitation must be carefully considered. For this reason, preliminary modal tests were completed first, during which piezoelectric discs were attached at different locations of the plate. These discs were utilized individually to provide separate excitation so that the levels of dynamic response could be compared, which would also verify the findings in the previous section. After this, the modal parameters were analyzed so that the frequency and location of excitation could be more properly selected for the subsequent vibrothermographic testing, increasing the possibility of successful damage detection.

In the experimental tests, the plate was suspended using two elastic bands connected to springs to simulate a free-free condition to avoid unnecessary external forces and constraints. In total, there were nine discs attached to the plate using superglue. However, only seven discs would be studied, which were discs D1, D3, D4, D5, D6, D7 and D8 in **Fig. 4**(b). Discs D2 and D9 were installed in a previous study for different purposes, so they were not related to this research.

As shown in **Fig. 4**(b), the piezoelectric discs were glued to brass substrates to form bending actuators. The diameters of the piezoelectric discs and the substrates were 15 mm and 20 mm respectively. The thickness was 0.2 mm each. The resonant frequency was around 6.8 kHz while the capacitance was 15000 pF (picofarad) $\pm 30\%$. Because of the amplitude and the frequency of excitation to be applied, an LDS PA100E power amplifier could be employed without needing more specialized equipment. As for data collection, a scanning laser Doppler vibrometer (SLDV) system was used to measure the vibration data while a Nippon Avionics TH9100MR infrared camera was employed to measure the temperature values.
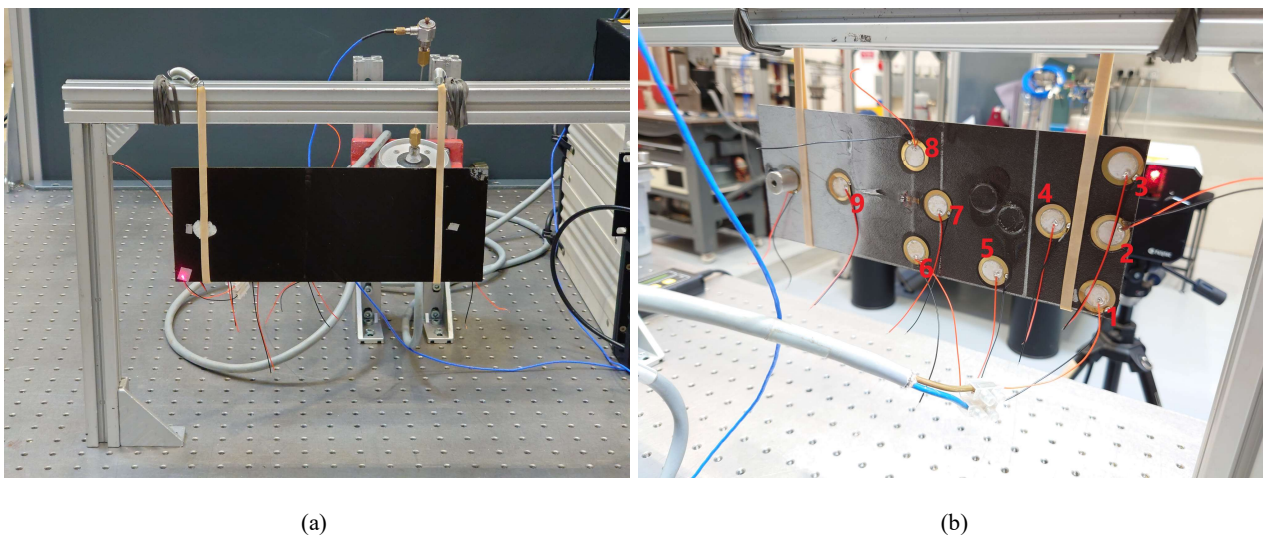

(a)   (b)

Fig. 4 The (a) rig set-up for the experimental tests on the composite plate and (b) locations of the piezoelectric discs

Before the experimental tests, an FE analysis was performed to predict the modal parameters of the plate, which would provide results at much higher resolutions. To achieve this, the composite plate was modelled as a 3D deformable shell using Abaqus built-in composite layup function based on the measured dimensions and the material properties provided by Hexcel and other sources [63, 64]. Zero boundary conditions were added in order to simulate the suspension of the plate in the experimental tests. A natural frequency extraction step was then performed, which yielded natural frequencies of 118.34 Hz, 374.32 Hz, 390.00 Hz, 746.44 Hz, 800.13 Hz and 1141.2 Hz for the first six modes of vibration. The mode shape and the distribution of strain energy of the first mode are presented in **Fig. 5** as examples.
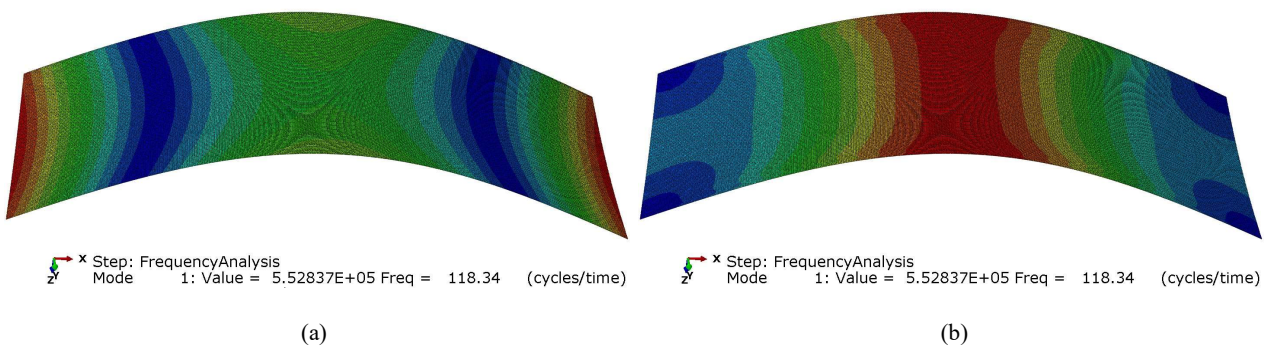

(a)   (b)

Fig. 5 (a) Mode shape and (b) distribution of strain energy of the first mode of the FE composite plate

To start the experimental tests, modal testing of the composite plate was conducted first to validate the FE model and to investigate the optimal location of excitation to increase the dynamic response level. In total, seven experimental modal tests were completed, each using a piezoelectric disc at a different location supplied with an input voltage of 30 V.

During the modal tests, a chirp signal sweeping from 20 Hz to 1000 Hz over 2 s was created to control the excitation. In each test, ten cycles of measurement were completed while the root mean square method was utilized to increase the signal-to-noise ratio. The frequency response functions (FRFs) were measured at the location indicated by the reflective tape with the red dot from the SLDV at the corner of the plate, as shown in **Fig. 4**(a). Based on the FRFs, the levels of dynamic response with different excitation locations could be compared.

After the modal tests, four modes of vibration were successfully discovered. However, the measured FRFs were heavily corrupted by noise, which was a consequence of the low power output of the piezoelectric discs. As demonstrations, the FRFs measured when discs D3 and D7 were used to excite the plate are shown in **Figs. 6**(a) and (b).
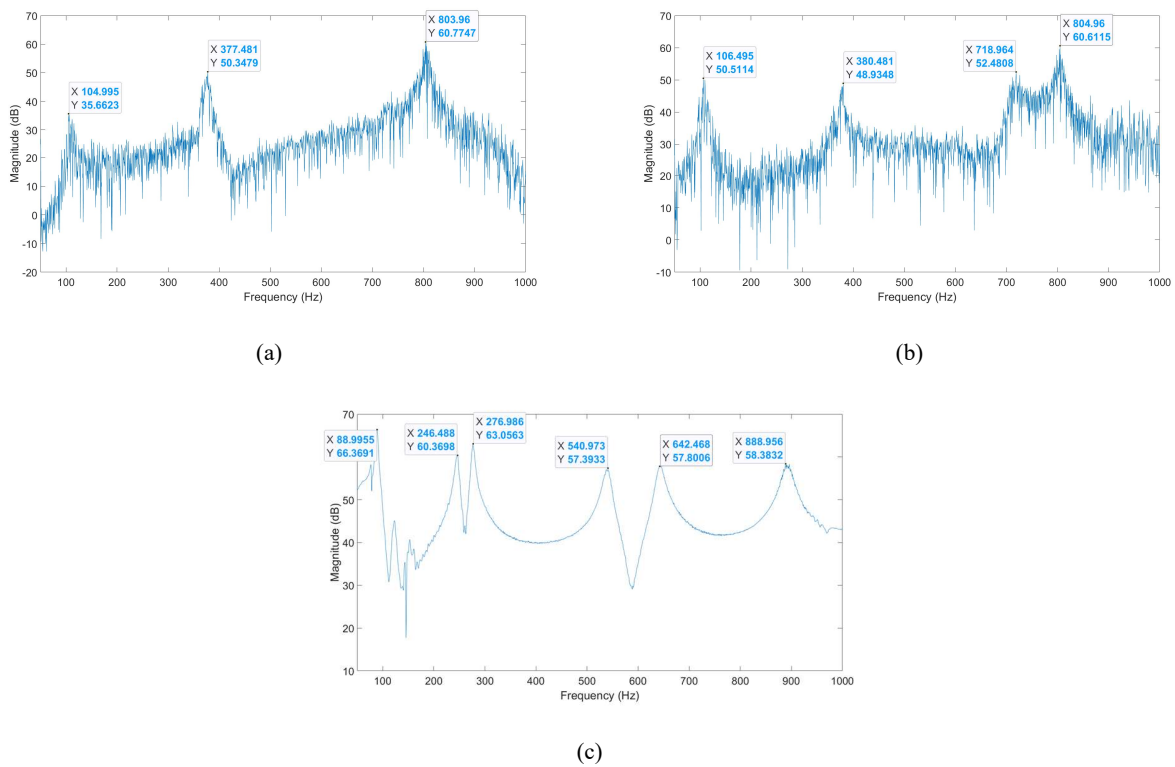

(a)

(b)

(c)

Fig. 6 Mobility plots when (a) piezoelectric disc D3, (b) piezoelectric disc D7 and (c) the LDS V201 shaker were utilized as the actuators

With the FRFs, the natural frequencies and the dynamic response levels were determined using peak picking. Due to the noise in the data, the values summarized in Table 1 were only approximate representations of the actual dynamic behaviors.

From the results in Table 1, it could be observed first that the natural frequencies measured here were close to those calculated from the FE analysis. However, the third mode of vibration observed in the FE analysis was unable to be detected here. Considering the quality of the data, it might be possible that it was mixed with the second mode and became indistinguishable. But based on the current data, it would be difficult to determine the exact reason behind its disappearance. It could also be assumed that this mode was not excited from the outset. Nevertheless, this phenomenon was relatively unimportant for the subsequent vibrothermographic testing as long as another mode with sufficient strain energy in the damaged region would exist and could be excited favorably.

Table 1: Natural frequencies (Hz) of the first five modes obtained through FE analysis as well as natural frequencies (Hz) and magnitude of dynamic response (dB) of the composite plate measured experimentally with each of the seven piezoelectric discs used as the actuator

Actuator	M. 1 freq. (mag.)	M. 2 freq. (mag.)	M. 3 freq. (mag.)	M. 4 freq. (mag.)	M. 5 freq. (mag.)
FE	118.34	374.32	390.00	746.44	800.13
D1	104.0 (32.3)	377.5 (48.8)	N/A	N/A	803.0 (55.4)
D3	105.0 (35.7)	377.5 (50.3)	N/A	N/A	804.0 (60.8)
D4	105.0 (32.3)	373.5 (59.5)	N/A	713.0 (52.8)	800.5 (54.3)
D5	109.5 (44.7)	379.0 (55.3)	N/A	717.0 (47.8)	807.0 (48.9)
D6	107.0 (47.7)	378.0 (59.9)	N/A	719.5 (54.5)	805.0 (48.0)
D7	106.5 (50.5)	380.5 (48.9)	N/A	719.0 (52.5)	805.0 (60.6)
D8	107.5 (51.3)	378.0 (64.7)	N/A	717.0 (54.2)	811.5 (62.8)

To demonstrate the relationship between the level of dynamic response and the local strain energy at the location of excitation, the first mode of vibration which was the first vertical bending mode could be studied because of its simple deflection shape. According to the distribution of strain energy shown in **Fig. 5**(b), locations closer to the center of the plate should have higher local strain energy. As marked in **Fig. 4**(b), this would correspond to discs with larger indices. From Table 1, it could be observed clearly that, for piezoelectric discs closer to the center of the plate, the levels of dynamic response were significantly greater when the first mode was targeted.

As a comparison, a final test was conducted using an LDS V201 permanent magnet shaker supplied with a 2 V voltage. The shaker was attached to the plate at the location marked by the metal connector in **Fig. 4**(b) through a drive rod. In contrast to the results with the piezoelectric discs, the FRF shown in **Fig. 6**(c) appeared significantly less noisy. The second and third modes of vibration, which were possibly mixed previously in **Figs. 6**(a) and (b) due to noise, were able to be distinguished. Quantitatively, the natural frequencies of the modes underwent noticeable decreases. This observation demonstrated the changes to the system's dynamic properties caused by the attachment of the drive rod and the shaker, which could be avoided by employing the lightweight piezoelectric discs as actuators instead.

By comparing **Figs. 6**(a), (b) and (c), the dynamic response levels of the first three modes were significantly higher using the shaker. For higher-order modes with natural frequencies greater than 500 Hz, the differences became smaller and eventually, a higher dynamic response level could be achieved with a piezoelectric disc. This phenomenon was able to corroborate that electrodynamic shakers are usually more suitable in low to medium frequency ranges while piezoelectric actuators often excel at higher frequencies.

VIBROTHERMOGRAPHIC TESTING
With the previous findings about the optimal location of excitation verified, the vibrothermographic tests could be initiated. From Table 1, regardless of the location of excitation, the level of dynamic response tended to be greater for higher-order modes of vibration, which was comprehensible due to the frequency response of the piezoelectric discs. Based on this observation, a relatively higher-order mode could be a more suitable target for vibrothermographic testing because of the higher heat generation caused by the greater dynamic response, in addition to the fact that a higher frequency of vibration itself would also accelerate the local heating.

Among the observed modes, the final mode had the highest natural frequency, which was around 800 Hz to 810 Hz. In this mode, there existed high local strain energy near the center of the plate which was where the damage was created, which was supported by the high dynamic response levels of this mode when discs D7 and D8 were used to excite the plate. This finding provided justification for the choice of using this mode for the vibrothermographic test. Despite the mode number, this frequency was still far from the typical high-frequency range that has been commonly applied in vibrothermography—which is often ultrasonic—so that the relevant issues discussed previously would not be encountered.

As for the location of excitation, although using disc D8 yielded the greatest dynamic response level as shown in Table 1, it was decided to employ disc D7 instead to avoid overlapping the location of excitation and the damage. To elaborate, during

the vibrothermographic test, heat would be emitted from the piezoelectric disc, so placing the disc at the location of the damage may cause the heat of the disc to be superimposed onto the heat generated due to the subsurface damage, complicating the analysis of the sources of the heat and hindering the detection of the damage.

To set up the test, a sinusoidal signal was generated at 810 Hz. The amplitude of the input voltage was set again to 30 V. During the vibrothermographic test, the TH9100MR infrared camera was set to capture one frame every 5 s. The test lasted for 22 min, so 265 frames of temperature data were recorded. The exact timeline of events is summarized in Table 2. The temperature recording began before the excitation started to measure the background data, which then continued after the excitation was stopped to capture the heat dissipation process. To present the results, eight representative images are shown in **Fig. 7**, in which a constant temperature scale from 24.7 ℃ to 25.7 ℃ was applied.

Table 2: Timeline of the events in the vibrothermographic test on the composite plate using the piezoelectric disc

Time (min:s)	Event
0:00	Data recording started
0:30	Infrared image displayed in **Fig. 7**(a) taken
2:00	Excitation turned on Infrared image displayed in **Fig. 7**(b) taken
3:00	Infrared image displayed in **Fig. 7**(c) taken
5:00	Infrared image displayed in **Fig. 7**(d) taken
7:00	Infrared image displayed in **Fig. 7**(e) taken
12:00	Excitation turned off Infrared image displayed in **Fig. 7**(f) taken
14:15	Infrared image displayed in **Fig. 7**(g) taken
22:00	Data recording stopped Infrared image displayed in **Fig. 7**(h) taken

Fig. 7(a) was taken at 30 s after the recording began, showing the initial temperature distribution. It could be observed that the spatial temperature variation on the composite plate was relatively small, mostly within the range of <0.2 ℃. This temperature variation should be attributed to the difference caused by the angle of view [65, 66].

Fig. 7(b) was taken 2 min after the recording began, which was the moment when the excitation was started. By comparing it with **Fig. 7**(a), the temperature distribution was generally unchanged, showing that no unexpected behaviors had happened.

The image in **Fig. 7**(c) was taken 1 min after the excitation was turned on, which was approximately the moment when the first visible local hot spot at the damage site was detected. As a comparison, this time—1 min—was significantly longer than its counterpart—which was only 4 s—in another test on the same plate using an LDS V201 permanent magnet shaker [1, 29]. For these reasons, it was evidenced that the heat generation was considerably lower using the piezoelectric disc.

The temperature and the corresponding thermal contrast of the hot spot continued to increase as more heat was generated. The continuous increase then gradually slowed and eventually, the characteristics of the hot spot were stabilized after approximately another 2 min, as shown in **Fig. 7**(d). In **Fig. 7**(d), the majority of the hot spot was only less than 0.5 ℃ hotter than the rest of the plate, noticeably lower than the values in the test using the shaker [1, 29].

After this event, the amplitude and size of the hot spot remained approximately unchanged. To support this observation, the images recorded at 7:00 and 12:00 of the test are displayed in **Figs. 7**(e) and (f). Visually, the overall temperature distributions and the characteristics of the hot spots looked almost identical. Only small discrepancies existed from **Fig. 7**(d) to **Fig. 7**(f), which should be attributed to the fluctuations caused by the slight inaccuracy of the infrared camera.

The input voltage was stopped at 12:00 of the test. It took approximately another 135 s for the local heat concentration to fully dissipate, as presented in **Fig. 7**(g). The final image taken before the recording was stopped, which was at 22:00 of the vibrothermographic test, is shown in **Fig. 7**(h). The similarity between **Figs. 7**(g) and **7**(h) indicated that no unexpected behaviors had happened after the excitation was stopped.
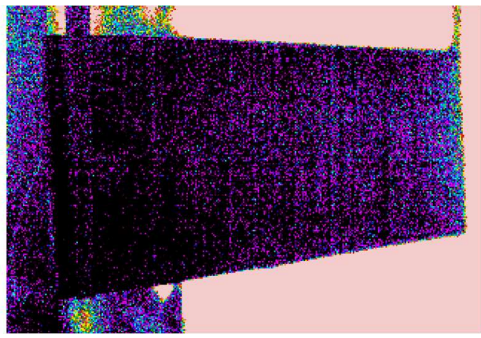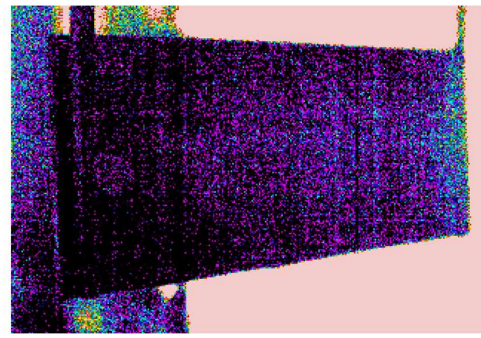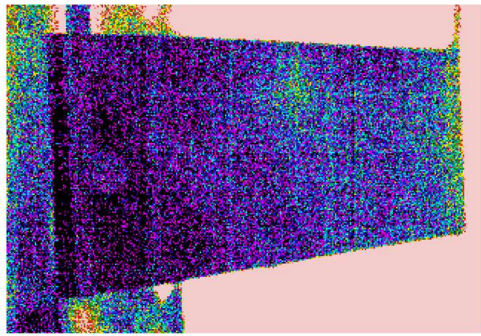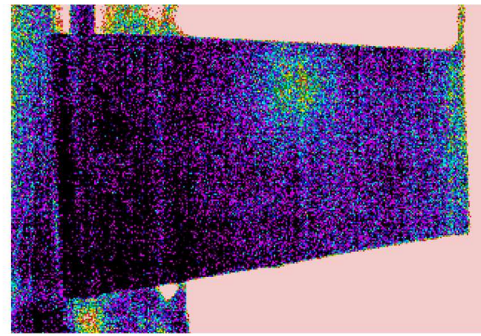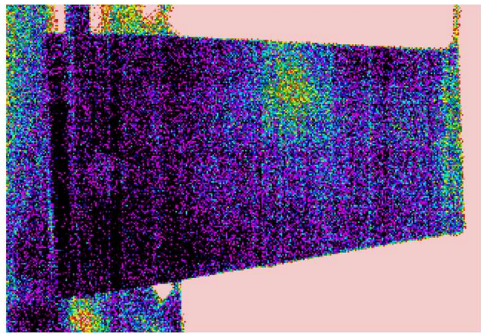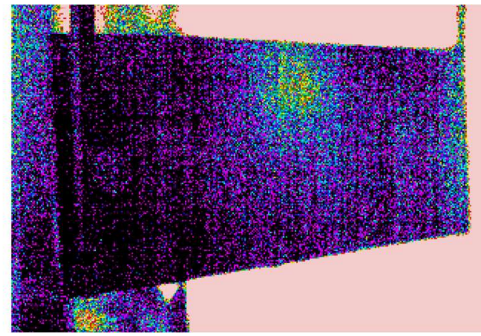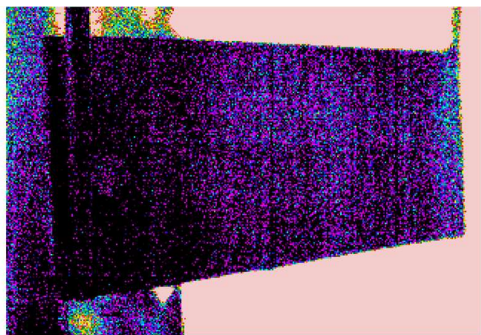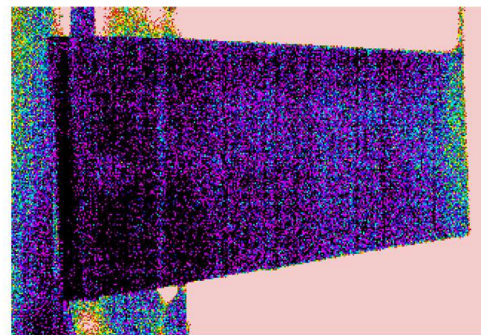
Fig. 7 Infrared images taken at (a) 0:30, (b) 2:00, (c) 3:00, (d) 5:00, (e) 7:00, (f) 12:00, (g) 14:15 and (h) 22:00 of the vibrothermographic test on the composite plate using the piezoelectric disc

With the completion of this vibrothermographic test showing the successful detection of the subsurface damage, additional tests were completed with different locations and frequencies of excitation. In these cases, the vibrothermographic tests were unable to yield equally positive results. Equally detectable heat could not be generated with these less optimal parameters.

Separately, an ultrasonic C-scan test was performed on this plate as additional verification [1, 29], showing that the vibrothermographic approach was able to identify and locate the damage successfully while having significant advantages in terms of measurement time. However, slight discrepancies were observed in terms of the size of the damage, which should be attributed to the low amplitude of excitation force that was unable to introduce sufficient relative movement and friction for the thermal pattern to reach its maximum potential size in the edge areas.
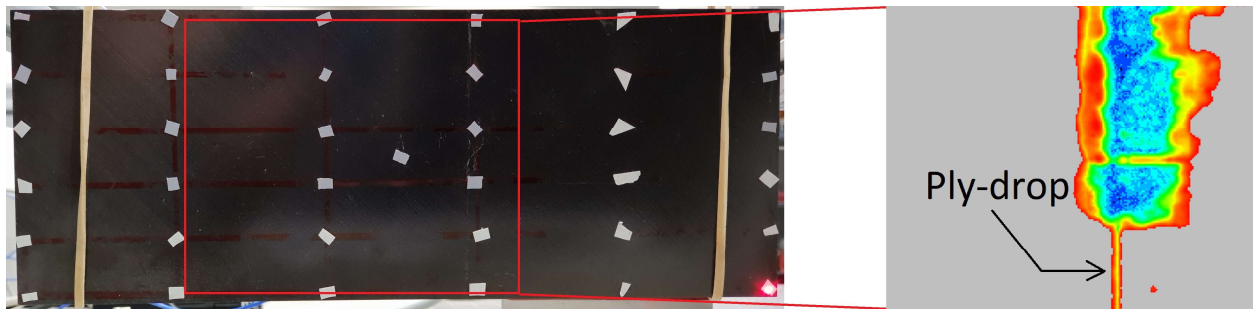

Fig. 8 Ultrasonic C-scan result of the central region of the composite plate

CONCLUSION

In the first part of the research, the optimal location of excitation using piezoelectric discs as actuators to increase the dynamic responses of structures was studied. Based on the results from the FE analyses, two generalized equations have been created to summarize the relationship between the excitation and the induced displacement response of the structure.

In the second part of the research, experimental modal analyses and vibrothermographic testing were completed on a composite plate using piezoelectric discs as actuators. During the modal tests, the conclusions made previously regarding the optimal location of excitation were verified experimentally. It was demonstrated that, despite the noise, the level of dynamic response was positively correlated with the local strain energy at the location of excitation. Based on this observation, the frequency and location of excitation could be selected for the subsequent vibrothermographic test.

In the vibrothermographic test, a visible hot spot was generated at the damage site under the vibration induced by a piezoelectric disc with carefully selected parameters of excitation. These results verified that low-power actuators such as the piezoelectric discs could be employed in vibrothermographic tests, providing benefits such as greater flexibility and less interference with the dynamic properties of the test structures. However, the parameters regarding the excitation of the structures must be more carefully selected to ensure sufficient levels of dynamic response and heat generation.

REFERENCES

[1] Chi, X., "Modal-based vibrothermography for damage detection and structural health monitoring," PhD thesis, University of Bristol, 2022.

[2] Renshaw, J., Chen, J. C., Holland, S. D., and Bruce Thompson, R., "The sources of heat generation in vibrothermography," *NDT & E International*, vol. 44, no. 8, pp. 736–739, 2011.

[3] Stinchcomb, W. W., *Mechanics of Nondestructive Testing*. Springer US, 1980.

[4] Henneke II, E. G., Reifsnider, K. L., and Stinchcomb, W. W., "Vibrothermography: Investigation, Development, and Application of a New Nondestructive Evaluation Technique," Engineering Science and Mechanics Department, Virginia Polytechnic Institute and State University Blacksburg, VA 24061, Tech report, 1986.

[5] Henneke II, E. G. and Jones, T. S., "Detection of Damage in Composite Materials by Vibrothermography," *Nondestructive Evaluation and Flaw Criticality for Composite Materials*, 1979.

[6] Henneke II, E. G., Reifsnider, K. L., and Stinchcomb, W. W., "Thermography — An NDI Method for Damage Detection," *JOM*, vol. 31, no. 9, pp. 11–15, 1979.

[7] Stepinski, T., Uhl, T., and Staszewski, W., *Advanced Structural Damage Detection: From Theory to Engineering Applications*. Wiley, 2013.

[8] Ibarra-Castanedo, C., Genest, M., Guibert, S., Piau, J.-M., Maldague, X. P. V., and Bendada, A., "Inspection of aerospace materials by pulsed thermography, lock-in thermography, and vibrothermography: a comparative study," in *Thermosense XXIX*, 2007, vol. 6541, pp. 321–329.

[9] Mignogna, R. B., Green, R. E., Duke, J. C., Henneke II, E. G., and Reifsnider, K. L., "Thermographic investigation of high-power ultrasonic heating in materials," *Ultrasonics*, vol. 19, no. 4, pp. 159–163, 1981.

[10] Montanini, R. and Freni, F., "Correlation between vibrational mode shapes and viscoelastic heat generation in vibrothermography," *NDT & E International*, vol. 58, pp. 43–48, 2013.

[11] Holland, S. D., Uhl, C., Ouyang, Z., Bantel, T., Li, M., Meeker, W. Q., Lively, J., Brasche, L., and Eisenmann, D., "Quantifying the vibrothermographic effect," *NDT & E International*, vol. 44, no. 8, pp. 775–782, 2011.

[12] Morbidini, M., Cawley, P., Barden, T., Almond, D., and Duffour, P., "Prediction of the thermosonic signal from fatigue cracks in metals using vibration damping measurements," *Journal of Applied Physics*, vol. 100, no. 10, p. 104905, 2006.

[13] Holland, S. D., Uhl, C., and Renshaw, J., "VIBROTHERMOGRAPHIC CRACK HEATING: A FUNCTION OF VIBRATION AND CRACK SIZE," *AIP Conference Proceedings*, vol. 1096, no. 1, pp. 489–494, 2009.

[14] Krapez, J.-C., Taillade, F., and Balageas, D., "Ultrasound-lockin-thermography NDE of composite plates with low power actuators. Experimental investigation of the influence of the Lamb wave frequency," *Quantitative InfraRed Thermography Journal*, vol. 2, no. 2, pp. 191–206, 2005.

[15] Solodov, I., Rahammer, M., Derusova, D., and Busse, G., "Highly-efficient and noncontact vibro-thermography via local defect resonance," *Quantitative InfraRed Thermography Journal*, vol. 12, no. 1, pp. 98–111, 2015.

[16] Bai, G., Lamboul, B., Roche, J.-M., and Baste, S., "Investigation of multiple cracking in glass/epoxy 2D woven composites by vibrothermography," *Quantitative InfraRed Thermography Journal*, vol. 13, no. 1, pp. 35–49, 2016.

[17] Kang, B. and Cawley, P., "Low Power PZT Exciter for Thermosonics," *AIP Conference Proceedings*, vol. 894, no. 1, pp. 484–491, 2007.

[18] Kang, B. and Cawley, P., "MULTI-MODE EXCITATION SYSTEM FOR THERMOSONIC TESTING OF TURBINE BLADES," *AIP Conference Proceedings*, vol. 975, no. 1, pp. 520–527, 2008.

[19] Kang, B., Lee, H., and Lee, C., "Performance of a small PZT exciter for thermosonic non-destructive testing," in *INTELEC 2009 – 31st International Telecommunications Energy Conference*, Oct. 2009, pp. 1–4.

[20] Renshaw, J., Holland, S. D., and Barnard, D. J., "Viscous material-filled synthetic defects for vibrothermography," *NDT & E International*, vol. 42, no. 8, pp. 753–756, 2009.

[21] Pye, C. J. and Adams, R. D., "Heat emission from damaged composite materials and its use in nondestructive testing," *Journal of Physics D: Applied Physics*, vol. 14, no. 5, pp. 927–941, 1981.

[22] Pye, C. J. and Adams, R. D., "Detection of damage in fibre reinforced plastics using thermal fields generated during resonant vibration," *NDT International*, vol. 14, no. 3, pp. 111–118, 1981.

[23] Homma, C., Rothenfusser, M., Baumann, J., Shannon, R., Thompson, D. O., and Chimenti, D. E., "Study of the Heat Generation Mechanism in Acoustic Thermography," *AIP Conference Proceedings*, vol. 820, no. 1, pp. 566–573, 2006.

[24] Rantala, J., Wu, D., and Busse, G., "Amplitude-modulated lock-in vibrothermography for NDE of polymers and composites," *Research in Nondestructive Evaluation*, vol. 7, no. 4, pp. 215–228, 1996.

[25] Harwood, N. and Cummings, W. M., *Thermoelastic Stress Analysis*. CRC Press, 1991.

[26] Morbidini, M., Cawley, P., Barden, T. J., Almond, D. P., and Duffour, P., "A New Approach for the Prediction of the Thermosonic Signal from Vibration Records," *AIP Conference Proceedings*, vol. 820, no. 1, pp. 558–565, 2006.

[27] Ewins, D. J., *Modal Testing: Theory, Practice and Application*, 2nd ed. Research Studies Press LTD, 2000.

[28] Meola, C., Boccardi, S., and Carlomagno, G. maria, *Infrared Thermography in the Evaluation of Aerospace Composite Materials*. Woodhead Publishing, 2015.

[29] Chi, X., Di Maio, D., and Lieven, N. A. J., "Modal-based vibrothermography using feature extraction with application to composite materials," *Structural Health Monitoring*, vol. 19, no. 4, pp. 967–986, 2020.

[30] Chi, X., Di Maio, D., and Lieven, N. A. J., "Health monitoring of bolted joints using modal-based vibrothermography," *SN Applied Sciences*, vol. 2, no. 8, 2020.

[31] Chi, X., Zhang, Y., Di Maio, D., and Lieven, N. A. J., "Viability of Image Compression in Vibrothermography," *Experimental Techniques*, vol. 45, no. 3, pp. 345–362, 2021.

[32] Chi, X., Di Maio, D., and Lieven, N. A. J., "Frictional heating as an estimator of modal damping and structural degradation: a vibrothermographic approach," in *12th Defence Science and Technology International Conference on Health and Usage Monitoring*, 2021

[33] Talai, S. M., Desai, D. A., and Heyns, P. S., "Infrared thermography applied to the prediction of structural vibration behaviour," *Alexandria Engineering Journal*, vol. 58, no. 2, pp. 603–610, 2019.

[34] Han, X., Zeng, Z., Li, W., Islam, Md. S., Lu, J., Loggins, V., Yitamben, E., Favro, L. D., Newaz, G., and Thomas, R. L., "Acoustic chaos for enhanced detectability of cracks by sonic infrared imaging," *Journal of Applied Physics*, vol. 95, no. 7, pp. 3792–3797, 2004.

[35] Favro, L. D., Han, X., Ouyang, Z., Sun, G., Sui, H., and Thomas, R. L., "Infrared imaging of defects heated by a sonic pulse," *Review of Scientific Instruments*, vol. 71, no. 6, pp. 2418–2421, 2000.

[36] Li, M., Holland, S. D., and Meeker, W. Q., "Quantitative Multi-Inspection-Site Comparison of Probability of Detection for Vibrothermography Nondestructive Evaluation Data," *Journal of Nondestructive Evaluation*, vol. 30, no. 3, pp. 172–178, 2011.

[37] Vaddi, J., Reusser, R., and Holland, S. D., "CHARACTERIZATION OF PIEZOELECTRIC STACK ACTUATORS FOR VIBROTHERMOGRAPHY," *AIP Conference Proceedings*, vol. 1335, no. 1, pp. 423–429, 2011.

[38] Vaddi, J., Holland, S. D., and Reusser, R., "Transducer degradation and high amplitude behavior of broadband piezoelectric stack transducer for vibrothermography," *AIP Conference Proceedings*, vol. 1430, no. 1, pp. 552–558, 2012.

[39] Vaddi, J. S., Holland, S. D., and Kessler, M. R., "Absorptive viscoelastic coatings for full field vibration coverage measurement in vibrothermography," *NDT & E International*, vol. 82, pp. 56–61, 2016.

[40] Demy, P., Golinval, J.-C., and Simon, D., "Damage detection in composites by vibrothermography and local resonances," *Mechanics & Industry*, vol. 14, no. 2, pp. 137–143, 2013.

[41] Holland, S. D., "First Measurements from a New Broadband Vibrothermography Measurement System," *AIP Conference Proceedings*, vol. 894, no. 1, pp. 478–483, 2007.

[42] Lamboul, B., Passilly, F., Roche, J.-M., and Balageas, D., "Ultrasonic vibrothermography using low-power actuators: An impact damage detection case study," *AIP Conference Proceedings*, vol. 1650, no. 1, pp. 319–326, 2015.

[43] Solodov, I., Bai, J., Bekgulyan, S., and Busse, G., "A local defect resonance to enhance acoustic wave-defect interaction in ultrasonic nondestructive evaluation," *Applied Physics Letters*, vol. 99, no. 21, p. 211911, 2011.

[44] Parvasi, S. M., Xu, C., Kong, Q., and Song, G., "Detection of multiple thin surface cracks using vibrothermography with low-power piezoceramic-based ultrasonic actuator—a numerical study with experimental verification," *Smart Materials and Structures*, vol. 25, no. 5, p. 055042, 2016.

[45] Zhu, L. and Guo, X., "Vibro-Thermography of Debonding Defects in Composite Plates," in *Conference on Quantitative Infrared Thermography – QIRT Asia 2017*. Daejeon, South Korea, 2017.

[46] Renshaw, J., Holland, S. D., and Bruce Thompson, R., "Measurement of crack opening stresses and crack closure stress profiles from heat generation in vibrating cracks," *Applied Physics Letters*, vol. 93, no. 8, p. 081914, 2008.

[47] Russell, S. S. and Henneke II, E. G., "Dynamic effects during vibrothermographic NDE of composites," *NDT International*, vol. 17, no. 1, pp. 19–25, 1984.

[48] Wang, C.-Y. and Yew, C. H., "Impact damage in composite laminates," *Computers & Structures*, vol. 37, no. 6, pp. 967–982, 1990.

[49] Bull, D. J., Spearing, S. M., Sinclair, I., and Helfen, L., "Three-dimensional assessment of low velocity impact damage in particle toughened composite laminates using micro-focus X-ray computed tomography and synchrotron radiation laminography," *Composites Part A: Applied Science and Manufacturing*, vol. 52, pp. 62–69, 2013.

[50] Yang, F. J. and Cantwell, W. J., "Impact damage initiation in composite materials," *Composites Science and Technology*, vol. 70, no. 2, pp. 336–342, 2010.

[51] Richardson, M. O. W. and Wisheart, M. J., "Review of low-velocity impact properties of composite materials," *Composites Part A: Applied Science and Manufacturing*, vol. 27, no. 12, pp. 1123–1131, 1996.

[52] Tai, N. H., Yip, M. C., and Lin, J. L., "Effects of low-energy impact on the fatigue behavior of carbon/epoxy composites," *Composites Science and Technology*, vol. 58, no. 1, pp. 1–8, 1998.

[53] Sjoblom, P. O., Hartness, J. T., and Cordell, T. M., "On Low-Velocity Impact Testing of Composite Materials," *Journal of Composite Materials*, vol. 22, no. 1, pp. 30–52, 1988.

[54] de Vries, E., "Mechanics and Mechanisms of Ultrasonic Metal Welding ," PhD thesis, The Ohio State University, 2004.

[55] Crawley, E. F. and de Luis, J., "Use of Piezoelectric Actuators as Elements of Intelligent Structures," *AIAA Journal*, vol. 25, no. 10, pp. 1373–1385, 1987.

[56] PI Ceramic, *Displacement Modes of Piezoelectric Actuators*. https://www.piceramic.com/en/piezo-technology/properties-piezo-actuators/displacement-modes. Accessed: 16/09/2022.

[57] Dimitriadis, E. K., Fuller, C. R., and Rogers, C. A., "Piezoelectric Actuators for Distributed Vibration Excitation of Thin Plates," *Journal of Vibration and Acoustics*, vol. 113, no. 1, pp. 100–107, 1991.

[58] Kim, T.-W. and Kim, J.-H., "Optimal distribution of an active layer for transient vibration control of a flexible plate," *Smart Materials and Structures*, vol. 14, no. 5, pp. 904–916, 2005.

[59] Ramesh Kumar, K. and Narayanan, S., "The optimal location of piezoelectric actuators and sensors for vibration control of plates," *Smart Materials and Structures*, vol. 16, no. 6, pp. 2680–2691, 2007.

[60] Aldraihem, O. J., Singh, T., and Wetherhold, R. C., "Optimal Size and Location of Piezoelectric Actuator/Sensors: Practical Considerations," *Journal of Guidance, Control, and Dynamics*, vol. 23, no. 3, pp. 509–515, 2000.

[61] Sadri, A. M., Wright, J. R., and Wynne, R. J., "Modelling and optimal placement of piezoelectric actuators in isotropic plates using genetic algorithms," *Smart Materials and Structures*, vol. 8, no. 4, pp. 490–498, 1999.

[62] Swann, C. and Chattopadhyay, A., "Optimization of piezoelectric sensor location for delamination detection in composite laminates," *Engineering Optimization*, vol. 38, no. 5, pp. 511–528, 2006.

[63] Hexcel Corporation, *HexPly® 8552 Epoxy Matrix Product Data Sheet*. 2020.

[64] Marlett, K., "Hexcel 8552S AS4 Plain Weave Fabric Prepreg 193 gsm & 38% RC Qualification Material Property Data Report," National Institute for Aviation Research, Wichita State University, Tech report, 2011.

[65] Speakman, J. R. and Ward, S., "Infrared thermography: principles and applications," *Zoology*, vol. 101, pp. 224–232, 1998.

[66] Nicodemus, F. E., "Directional Reflectance and Emissivity of an Opaque Surface," *Applied Optics*, vol. 4, no. 7, pp. 767–775, 1965.